Journal Pre-proof

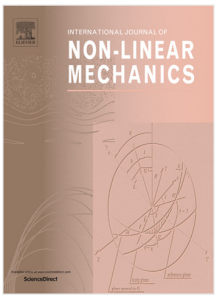

Performance boost of an electromagnetic energy harvester using vibrational resonance

K.A. Omoteso, T.O. Roy-Layinde, U.H. Diala

PII: S0020-7462(24)00354-8
DOI: https://doi.org/10.1016/j.ijnonlinmec.2024.104989
Reference: NLM 104989

To appear in: *International Journal of Non-Linear Mechanics*

Received date : 21 October 2024
Revised date : 26 November 2024
Accepted date : 10 December 2024

Please cite this article as: K.A. Omoteso, T.O. Roy-Layinde and U.H. Diala, Performance boost of an electromagnetic energy harvester using vibrational resonance, *International Journal of Non-Linear Mechanics* (2024), doi: https://doi.org/10.1016/j.ijnonlinmec.2024.104989.

Performance boost of an electromagnetic energy harvester using vibrational resonance

K.A. Omoteso[a], T.O. Roy-Layinde[b], U.H. Diala[a,*]

[a] *School of Engineering, University of Derby, Markeaton Street, Derby, United Kingdom*
[b] *Department of Physics, Olabisi Onabanjo University, Ogun State, Nigeria*

Abstract

Inherent nonlinearities, present in dynamical systems are employed to solve various engineering problems. Nonlinear dynamics involve responses that are not directly proportional to inputs, allowing for more effective system management. The beneficial characteristics of nonlinear systems and its growing associated literature have contributed to mitigating industrial and environmental energy-related challenges. Several recommendations have been provided for increasing the efficiency of a vibration energy harvesting (VEH) system. In this study, we investigated the occurrence of vibrational resonance (VR) in a Duffing-type energy harvester with electromagnetic transduction structure. We explored the impact of system nonlinearities on the occurrence of VR and system performance. We employed both analytical and numerical approaches to show the impact of the system parameters, especially the nonlinear stiffness parameter on the response amplitude at low-frequency excitations. Furthermore, the estimated average power absorbed by the VEH system is selected as the system performance metric, which can be optimised using the system's parameters of interest. The VEH system demonstrated an improved performance as a significant amount of energy was harvested based on the nonlinear parameters of interest. Our investigation points to a new approach for the design and optimization of electromagnetic energy harvester.

Keywords: Nonlinear systems, Bi-harmonics, Vibrational resonance, Vibration Energy Harvester, Average power.

1. Introduction

Ambient energy harvesting such as vibration, heat, and acoustic energy harvesting is receiving significant attention from the research community. This is majorly as a result of the global drive to reduce carbon emissions due to its detrimental effect on the ecosystem and the environment. These ambient energies can be harvested using several techniques such as acoustic energy harvesting (AEH), thermoelectric energy harvesting (TEH), triboelectric nanogenerator (TENG), and vibration energy harvesting (VEH) [1, 2]. It should be noted that VEH encompasses piezoelectric energy harvesting, electromagnetic energy harvesting, and electrostatic energy harvesting [3, 4]. Generally, vibration energy harvesters are systems that transform vibration energy into electrical energy [1, 2, 5, 6].

Studies on vibration energy harvesting have presented diverse perspectives regarding the potential conversion of mechanical oscillations into electrical energy. Linear VEH systems are designed to harvest maximum energy at their natural frequencies. However, to extend the frequency range over which energy can be harvested, nonlinear parameters (specifically, stiffness nonlinearities) are integrated into the system. This is implemented either geometrically [7], structurally [4, 8], or inherently [9, 10]. Meanwhile, in order to maximize the energy harvested, the VEH system is designed to match the dominant frequency of the environmental vibration. In general, less energy is harvested because most mechanical harvesters have a narrow bandwidth and a complicated resonant frequency-matching process.

Several studies on improving the performance of a VEH system employed the traditional single-degree-of-freedom mechanical system, including its beam-type variants [3]. VEH systems have benefited from the application of nonlinear analytical methods, since most physical systems are inherently nonlinear. For this reason, it is important to consider the impact of nonlinear parameters, on the performance of a VEH system. For instance, bistable energy harvesters extract more energy when its nonlinear characteristics are considered [4, 10, 11, 12]. Also, nonlinearly damped VEH systems extract the same amount of energy as its equivalent linearly damped system at maximum excitations, but performs better at excitation levels below the maximum level [11]. In a study on the influence of internal resistance on an energy harvester with a damping system modeled as a nonlinear cubic load, it was shown that a VEH system's dynamic range could be extended by varying the load resistance, thereby improving the output power absorbed in the process [10].

Nonlinear phenomenology is beneficial in improving the performance of VEH systems, as recently shown in a Duff-

*Corresponding author tel. no: +447477445446
Email address: U.Diala@derby.ac.uk (U.H. Diala)

ing oscillator with cubic damping in [5]. For instance, many studies focused on modulating the dynamical systems' nonlinearities to improve a Duffing oscillator-based VEH system design, it was observed that under specific harmonic forcing the system's performance was optimized, for both potentially stable and nonlinear monostable scenarios [2, 12, 13]. All VEH systems exhibit some degree of intrinsic nonlinearity, which may be structural, geometric or frictional [4, 7, 8]. Diala *et al.,* in [14], showed the impact of a nonlinear hardening spring with cubic damping on a VEH system, assuming no restriction on the maximum throw, using a frequency-based analytical tool, the Output Frequency Response Function (OFRF), derived using the Associated Linear Equations (ALEs) of the system model. In the study, the methodology employed yielded the best possible parameter values for the VEH system design to yield the desired output energy. The performance of a VEH system can be enhanced by integrating a nonlinear cubic stiffness parameter to the system, which is capable of widening the bandwidth over which energy can be harvested as demonstrated in [14, 12].

It has been established in literature that nonlinearity can be implemented using several geometric arrangements, to achieve a simultaneous passive vibration suppression and energy harvesting [7, 15, 16]. For instance, a nonlinear dual-function multi-modal energy harvester and vibration absorber (EHVA) for harvesting energy and suppressing vibration in the low–medium frequency band was reported in [16]. The design of the multi-modal shapes of the EHVA, as well as the hysteresis property of nonlinear softening springs were the two primary methods employed by the authors to extend the operational frequency of the system. In [17], Wang and Zhu connected a magnetic multi-stable device to a pendulum VEH, to increase its bandwidth, particularly while operating at low frequencies. A theoretical and experimental investigation into the design of a magnetic spring based on a nonlinear electromagnetic converter was carried out in [18]. The magnetic force acting on the moving magnet was specifically examined in the study, taking into account two factors; the magnets' volume and the two fixed magnets' shapes. Recently, a magnetic-spring-based electromagnetic energy harvester with piecewise nonlinear stiffness was numerically investigated in [19]. It was shown that the piecewise nonlinear stiffness behaviour (magnetic flux), which was created as a result of the interaction of the moving magnet with the coil allowed the system to respond over a larger frequency range and produce more electrical energy. The foregoing scores the fact that much effort has been directed towards the development of effective devices that can work well over a larger bandwidth, through nonlinearities.

Nonlinear dynamical systems are also known to undergo nonlinear resonances, and the resonant behaviours can be improved through system parameters [20]. For example, in [21], the authors reported a double-jump phenomenon when examining the steady-state response of a particular VEH system in the presence of both internal and external resonance. The frequency response curve demonstrates the presence of resonance peaks that shifted to the left and /or right of the system's natural frequency. Various external factors such as random environmental excitation, which leads to the occurrence of other nonlinear resonant behaviours in VEH systems can be used to improve the performance of energy harvesters [22, 23, 24, 25, 26]. The response of a bistable energy harvester with symmetric potential under random environment excitation was studied in [27], proving the mean-square voltage can be raised by intensifying Gaussian white noise. The energy harvesting capabilities of nonlinear vibrational multistable energy harvesters was impacted by stochastic bifurcation phenomena caused by narrow-band stochastic parametric stimulation [25]. Recently, the occurrence of stochastic resonance (SR) in a bistable piezoelectric harvester subjected to additive Gaussian white noise and harmonic excitation was reported in [26]. They established that stochastic resonance can be utilised to improve the performance of energy harvesters.

Vibrational resonance (VR) [28, 29, 30], which is an example of nonlinear resonance similar to stochastic resonance, generally occurs when a high-frequency harmonic signal plays the role of noise in SR. VR typically occurs in dual-frequency-driven nonlinear systems with distinct frequencies [28, 31, 32]. In VR, a nonlinear system driven by a low-frequency (ω) signal is typically excited by a second, higher-frequency (Ω) harmonic forcing, known as the fast-signal, with $\Omega \gg \omega$. The system's response amplitude, at the slow oscillation frequency is calculated as a function of the fast signal's amplitude, and the resulting curve resembles the well-known signal-to-noise ratio curves found in stochastic resonance (SR) [33, 29, 30]. VR has been adopted for a wide range of real-world applications in engineering, as well as pure and applied sciences. Most recently, in [34], VR was utilised to study the motion of air particles in the cavity of a Helmholtz resonator (HR), excited by a dual-frequency acoustic wave. The low-frequency (LF) signal in the acoustic field was amplitude-modulated by an additive high-frequency (HF) perturbation, which enhanced the detection of the LF through VR phenomena. The results provided insights to the design of improved acoustic resonators, an efficient passive sound controller that finds application in different engineering designs, especially in simultaneous noise attenuation and acoustic energy harvesting. Also, the electrical response of a double-well Duffing oscillator coupled to a circuit through piezoceramic elements, driven by a bi-harmonic forcing function was enhanced through the phenomenon of vibrational resonance [1]. In a subsequent study, the same authors demonstrated that more electrical energy could be gained by increasing the oscillations and that the amplification effects could be precisely regulated [35].

Generally, there are several challenges with the operation of VEH systems in an environment with higher harmonics. To capture all the active spectrum and multiple frequency shifts for vibration scenarios with higher fre-

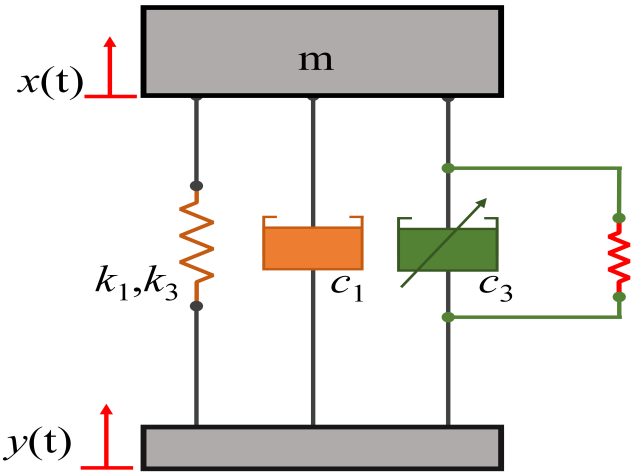

Figure 1: The SDOF vibration energy harvester with nonlinearly damper.

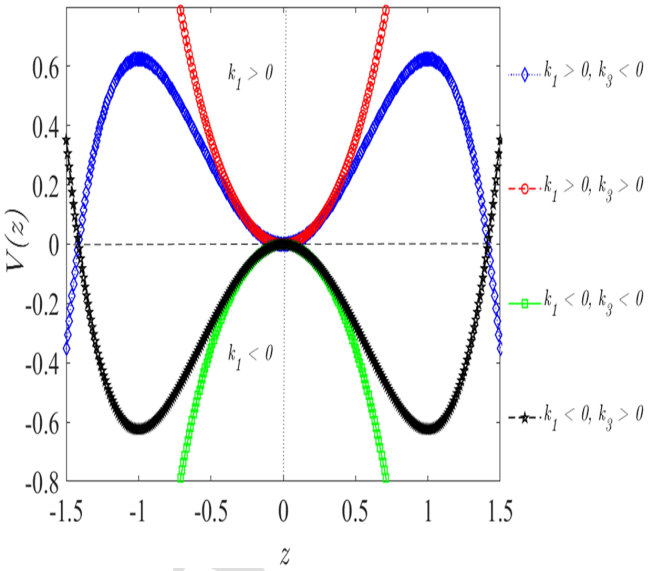

Figure 2: The potential structure of the modeled SDOF energy harvester computed from Eq. (7) for different sign combinations of k_1 and k_3

quencies found in motors, engineering structures, infrastructural assets with truss, tunnels and rail bridges [36], which limits the performance of VEH system to a specific application, there is a compelling need for further investigation of the nonlinear responses of a weakly driven VEHs to the effects of high-frequency components. We under take such investigation here, and explore the nonlinear features of the energy harvester to maximise the system's performance. In this study, we investigate the VR phenomenon in a dual-frequency driven nonlinear system modeling an electromagnetic energy harvester, where to the best of our knowledge, the influence of a high-frequency excitation on a weakly-driven harvester has not been reported [30]. The rest of this paper is organised as follows: Section 2 describes the VEH system model. The behaviour of the VEH system is investigated analytically and numerically using the VR method in Section 3. The dynamical response of the system is discussed in Section 4. Numerical simulation of the average power generated by the vibration energy harvester is presented in Section 5, while the paper is concluded in Section 6.

2. Model Description

The model under consideration is a vibration-based energy harvester with a single degree of freedom (SDOF), presented in Fig. 1. It has an isolated mass m, and base displacement of $y(t)$. The system consists a parallel combination of nonlinear stiffness and damping components separating the mass from the base. The damper has linear and nonlinear damping coefficients c_1 and c_3, respectively, and the stiffness has linear and nonlinear coefficients k_1 and k_3, respectively. The SDOF VEH system model shown in Fig. 1 is described by a nonlinear differential equation (NDE) of motion given by

$$m\ddot{z} + c_1\dot{z} + c_3\dot{z}^3 + k_1 z + k_3 z^3 = m\ddot{y}, \tag{1}$$

where $x(t)$ denotes the mass's absolute displacement and m is the isolated constant mass m. The relative displacement between the spring mass and the base-support is denoted by $z(t) = x(t) - y(t)$. The base displacement is assumed to be harmonic with amplitude Y and frequency ω, and its expressed in the absence of a phase difference as

$$y = Y\sin(\omega t). \tag{2}$$

In order to enhance the VEH's performance using VR, the base displacement $y(t)$ is assumed to be an additive biharmonic forcing comprising an imposed high-frequency forcing with frequency Ω and a weak low-frequency signal with frequency ω, so that Eq. (2) becomes

$$y = Y(\sin(\omega t) + g\sin(\Omega t)), \tag{3}$$

and Eq. (1) becomes

$$\begin{aligned} m\ddot{z} \quad &+ \quad c_1\dot{z} + c_3\dot{z}^3 + k_1 z + k_3 z^3 = Ym\omega^2\sin(\omega t) \\ &+ \quad gYm\Omega^2\sin(\Omega t) \end{aligned} \tag{4}$$

$Ym\omega^2\sin(\omega t)$ is the slow forcing and $gYm\Omega^2\sin(\Omega t)$ is the fast periodic excitations with a high frequency. By re-scaling the variables in Eq. (4) using

$$\begin{aligned} \alpha \quad &= \quad \frac{c_1}{m}, \quad \beta = \frac{c_3}{m}, \quad \gamma_1 = \frac{k_1}{m}, \quad \gamma_2 = \frac{k_3}{m}, \\ f \quad &= \quad Y\omega^2, \quad F = gY\Omega^2, \end{aligned} \tag{5}$$

with a constant-unity mass ($m = 1$), the non-dimensional equation of motion, Eq. (4), can be written in the form

$$\ddot{z} + \alpha\dot{z} + \beta\dot{z}^3 + \gamma_1 z + \gamma_2 z^3 = f\sin(\omega t) + F\sin(\Omega t). \tag{6}$$

The VEH system's potential $V(z)$ is given by

$$V(z) = \frac{\gamma_1}{2}z^2 + \frac{\gamma_2}{4}z^4. \quad (7)$$

The system's potential, Eq. (7) possesses three equilibrium points ($P_{1,2,3}(z^*, y^*)$). These points depend on the signs and values of γ_1 and γ_2, which are determined by the two stiffness parameters k_1 and k_3, respectively. The potential shape of a typical Duffing oscillator can be represented in four different ways depending on the signs of the stiffness coefficients k_1 and k_3 [20].

The four potential structures are shown in Fig. 2. If the two stiffness parameters have same signs, the system exhibits a single-hump (for $k_1 < 0,\ k_3 < 0$) and a single-well (for $k_1 > 0,\ k_3 > 0$) potential shapes. These yield identical trivial equilibrium points which are zero and imaginary values, $P_1(0,0)$ and $P_{2,3}(\pm i\sqrt{\frac{k_1}{k_3}}, 0)$. The single-hump potential structure for $k_1 \leq k_3 < 0$ is of no physical consequence [20]. This is because the associated equilibrium point, $P_1(0,0)$ is highly unstable, and P_2 and P_3 are imaginary points. The equilibrium point $P_1(0,0)$ obtained for the positive stiffness parameters ($k_1,\ k_3 > 0$) is stable and significant. The three cases of the system's potential with at least one of the parameters greater than zero, particularly, $k_1 > 0$, have evolved into a traditional central paradigm for explaining nonlinear events. These facilitate resonance analysis, especially nonlinear resonance behaviours [20, 37, 38]. With k_1 and k_3 having different signs (e.g. $k_1 < 0$ and $k_3 > 0$), the system exhibits a double-well-single-hump potential structure. It exhibits real equilibrium points $P_1(0,0), P_{2,3}(\pm\sqrt{\frac{k_1}{k_3}}, 0)$. Also, the potential is single-well-double-hump for $k_1 > 0$ and $k_3 < 0$. In summary, the following conditions define the potential structure of the system;

i. a single-well with the minimum at $z = 0$, when $k_3 \geq k_1 > 0$.

ii. a double-well-single-hump structure with a local maximum at $z = 0$ and two minima at $z = \pm\sqrt{\frac{|k_1|}{k_3}}$, for $k_1 < 0 < k_3$.

iii. an inverted single-well (single-hump) that has its maximum at $z = 0$ when $k_1 \leq k_3 < 0$.

iv. a double-hump-single-well structure with a maximum at $z = 0$ and two minima at $z = \pm\sqrt{\frac{k_1}{|k_3|}}$, for $k_3 < 0 < k_1$.

For this study, we consider the response of the VEH system within the single-well potential condition ($k_3 > 0$ and $k_1 > 0$). To explore the impact of the nonlinear stiffness on the system's dynamics, we observe the influence of k_3 on the effective potential of the system as shown in Fig. 3a. From the figure, increased hardening stiffness, k_3, decreases the potential width, and thus increases the stability of the system's particles. This is because the effect of the perturbation increases the amount of energetic particles oscillating around the equilibrium point ($z = 0$), imposing a high possibility of overcoming the impact of obstacles along their trajectories [39]. In other words, the increased nonlinear stiffness energizes the particles systematically and minimizes the effect of dynamical barriers on the system. Therefore, it enhances the performance threshold of the vibration energy harvester. This implies that the high periodicity of the system's oscillations optimizes the overall performance of the system. Despite the increased stability condition, the possibility of observing multiple resonances, in the context of vibrational resonance with the Duffing oscillator, for the single-well potential condition is prevented by the monotonic increase in the resonance frequency [20]. However, our focus will be to explore the dynamical response of the VEH system within a suitable parameter regime that optimizes the system's performance.

3. Resonance Dynamics of the VEH system

3.1. Analytical description

To analytically analyse the occurrence of vibrational resonance in the biharmonically driven VEH oscillator given in Eq. (6), we use the method of direct separation of motions (MDSM) [30, 37, 40].

When used alone or in conjunction with other perturbation techniques, the MDSM is a useful mathematical tool for examining the effects of a high-frequency excitation in oscillators [41, 42, 43, 44, 45]. The method involves splitting the vibration of the oscillatory system into a set of integro-differential equations. One of the equations describes the slow motion of the system whose response can be modulated by varying the parameters of the high-frequency field, and the other describes the fast motion. The response of the VEH system is characterized by the computation of a response amplitude, Q, given as the ratio of the amplitudes A_L of the oscillating system to that of the weak signal, f.

Generally, the mechanical system given by Eq. (6) can be expressed in the form:

$$m\ddot{z} = F(\dot{z}, z, t) + \Phi(\dot{z}, z, t, \omega t). \quad (8)$$

The solution $z(t)$ of Eq. (6) or its general form, system (8) consists of a superposition of only the solutions $h(t)$ of slow evolution with frequency ω and $H(t,\tau),\ \tau = \Omega t$ of the fast oscillations with frequency Ω when $\Omega \gg \omega$. That is,

$$z(t) = h(t) + H(t, \Omega t). \quad (9)$$

where $h(t)$ is assumed to be periodic with period $T = \frac{2\pi}{\omega}$ and H is periodic in the fast time $\tau = \Omega t$ with period 2π. The goal is to derive a system of two-coupled integro-differential describing the system's dynamics in h and H from the main equation of the system (Eq. (6)). We will then focus on the equation of the slow component which gives information on how the parameters of the fast signal

influence the system's dynamics. Moreover, the average value of $H(t,\tau)$, i.e. $\langle H(t,\tau)\rangle$ with respect to fast time τ is given by

$$\langle H(t,\tau)\rangle = \overline{H}(t,\tau) = \frac{1}{2\pi}\int_0^{2\pi} H(t,\tau)dt = 0. \quad (10)$$

Based on Eq. (8) and the assumed solution in Eq. (9), the two coupled system of integro-differential equations are

$$\begin{aligned} m\ddot{h} &= F(\dot{h},h,t) + \langle\hat{F}(\dot{h},h,\dot{H},H,t)\rangle \\ &+ \langle\Phi(\ddot{h}+\ddot{H},\dot{h}+\dot{H},h+H,t,\tau)\rangle, \end{aligned} \quad (11)$$

and

$$\begin{aligned} m\ddot{H} &= \hat{F}(\dot{h},h,t) - \langle\hat{F}(\dot{h},h,\dot{H},H,t)\rangle + \Phi(\ddot{h} \\ &+ \dot{H},h+H,t,\tau) - \langle\Phi(\ddot{h}+\ddot{H},\dot{h}+\dot{H},h+H,t,\tau)\rangle, \end{aligned} \quad (12)$$

where

$$\hat{F}(\dot{h},h,\dot{H},H,t) = F(\dot{h}+\dot{H},h+H,t) + F(\ddot{h},h,t). \quad (13)$$

Equation (13) is the function of the system's variables, from which one can compute the response amplitudes Q of the system. If h and H are the solutions of Eq. (11) and Eq. (12), respectively, it implies that $z = h+H$ is the solution of the general Eq. (8).

The first of the coupled integro-differential equations (Eq. 11) is obtained by substituting Eq. (9) into Eq. (8), and averaging both sides of with respect to the fast time τ in accordance with Eq. (10). The second Equation (Eq. 12) is derived by subtracting the first equation (Eq. 11) from the general equation of the system (Eq. (8)). In Equation (12), $\dot{h}$ and h frozen, that is, constant since the H component is faster than the slow component h.

Following the acquisition of a solution $H = H^*(\dot{h},h,t,\tau)$, it becomes evident that Eq. (11) can be expressed as

$$m\ddot{h} = F(\dot{h},h,t) + V(\dot{h},h,t), \quad (14)$$

where

$$\begin{aligned} V(\dot{h},h,t) &= \langle\hat{F}(\dot{h},h,\dot{H}^*,H^*,t)\rangle + \langle\Phi(\ddot{h}+\dot{H}^*,h \\ &+ H^*,t,\tau)\rangle. \end{aligned} \quad (15)$$

For the fast component H^*, one will typically need to look for an approximate solution in the form of a few harmonics. It is possible to find a solution by linearising F and Φ with regard to H (and maybe $\dot{h}$) if H is thought to be modest in relation to h.

The MDSM has been explained in detail in Refs. [20, 46], and effectively applied for a variety of theoretical VR analyses [47, 48, 49, 50, 51, 52, 53, 54].

In order to ensure that the potential $V(z)$ is well-defined over a specific range of initial conditions of the fast variables H, we assume that the fast motion H^* is asymptotically constant throughout our analysis of VR in this paper. The potential $V(z)$ will vary depending on which of the several steady rapid motions is taken into consideration. Eq. 14 is the primary equation for the study of the system's vibrational mechanics [46]. The slow dynamics equation has an effective potential because of the fast dynamics.

Therefore, to apply MDSM, one can substitute Eq. (9) into Eq. (6), to have

$$\begin{aligned} \ddot{h} &+ \ddot{H} + \alpha(\dot{h}+\dot{H}) + \beta(\dot{h}+\dot{H})^3 + \gamma_1(h+H) \\ &+ \gamma_2(h+H)^3 = f\sin(\omega t) + F\sin(\Omega t). \end{aligned} \quad (16)$$

Averaging both sides of Eq. (16) over the period of fast time $[0,\ \frac{2\pi}{\Omega}]$ gives

$$\begin{aligned} \ddot{h} &+ \overline{\ddot{H}} + \dot{h}(\alpha + 3\beta\overline{\dot{H}^2}) + \alpha\overline{\dot{H}} + 3\overline{\ddot{H}}h^2 + \beta\dot{h}^3 + \beta\overline{\dot{H}^3} \\ &+ h(\gamma_1 + 3\gamma_2\overline{H^2}) + \gamma_1\overline{H} + 3\gamma_2\overline{H}h^2 + \gamma_2h^3 + \gamma_2\overline{H^3} \\ &= f\sin(\omega t) + \overline{F\sin(\Omega t)}. \end{aligned} \quad (17)$$

By applying the mean value in Eq. (10) in Eq. (17), Eq. (17) becomes

$$\begin{aligned} \ddot{h} &+ \dot{h}(\alpha + 3\beta\overline{\dot{H}^2}) + \beta\dot{h}^3 + \beta\overline{\dot{H}^3} + h(\gamma_1 + 3\gamma_2\overline{H^2}) \\ &+ \gamma_2h^3 + \beta\overline{H^3} = f\sin(\omega t). \end{aligned} \quad (18)$$

Eq. (18) is the first of the set of coupled equations we set out to obtain. It is the integro-differential equation for the slow variable h. The equation of the fast oscillatory motion is obtained by subtracting Eq. (18) from Eq. (16), to obtain

$$\begin{aligned} \ddot{H} &+ 3\beta\dot{h}(\dot{H}^2 - \overline{\dot{H}^2}) + \alpha\dot{H} + 3\dot{H}\dot{h}^2 + 3(\ddot{H}^3 - \overline{\ddot{H}}) \\ &+ \beta\dot{H}^3 + \gamma_1H + 3\gamma_2h(H^2 - \overline{H^2}) + 3\gamma_2\overline{H}h^2 \\ &+ \gamma_2(H^3 - \overline{H^3}) = F\sin(\Omega t). \end{aligned} \quad (19)$$

Using the inertial approximation by assuming $\ddot{H} \gg \dot{H} \gg H$, we can write the approximate form of Eq. (19) as

$$\ddot{H} = F\sin(\Omega t), \quad (20)$$

so that

$$H = \frac{-F}{\Omega^2}\sin(\Omega t), \quad (21)$$

Using Eq. (21), the mean values in Eq. (18) are obtained as

$$\begin{aligned} \overline{\dot{H}^2} &= \frac{F^2}{2\Omega^2}, \qquad \overline{H^2} = \frac{F^2}{2\Omega^4}, \qquad \overline{H^4} = \frac{3F^4}{8\Omega^8}, \\ \overline{\dot{H}^3} &= 0, \ \ \overline{H} = \overline{H^3} = \overline{H^5} = \overline{H^7}... = 0. \end{aligned} \quad (22)$$

By substituting Eq. (22) into Eq. (18), we obtain

$$\begin{aligned} \ddot{h} &+ \dot{h}(\alpha + 3\beta\frac{F^2}{2\Omega^2}) + \beta\dot{h}^3 + h(\gamma_1 + 3\gamma_2\frac{F^2}{2\Omega^4}) \\ &+ \gamma_2h^3 = f\sin(\omega t). \end{aligned} \quad (23)$$

Eq. (23) can be written as

$$\ddot{h} + \dot{h}\lambda_1 + \beta\dot{h}^3 + \lambda_2h + \gamma_2h^3 = f\sin(\omega t), \quad (24)$$

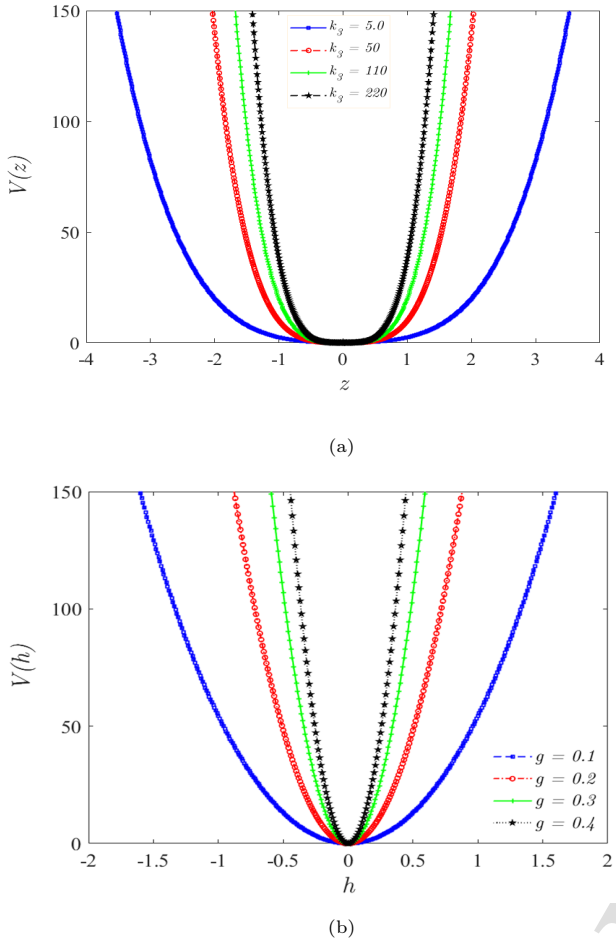

Figure 3: (a) Potential plots of the VEH system, $V(z)$ against displacement, z with varying values of the nonlinear stiffness parameter, k_3 when $k_1 = 5$. (b) The effective potential plots, $V(h)$ against h, for different values of g, magnitude of the fast oscillation with other parameters fixed at $k_1 = 5,\ k_3 = 5,\ \omega = 1.0,\ \Omega = 20\omega$.

where

$$\begin{aligned} \lambda_1 &= \alpha + 3\beta\frac{F^2}{2\Omega^2}, \\ \lambda_2 &= \gamma_1 + 3\gamma_2\frac{F^2}{2\Omega^4}. \end{aligned} \tag{25}$$

Thus, the effective potential of the system is given by

$$V(h) = \frac{\lambda_2}{2}h^2 + \frac{\gamma_2}{4}h^4. \tag{26}$$

Figure 3 presents the effective potential $V(h)$ as a function of the slow motion component, h and Fig. 3b shows the effect of increasing g on the system's potential. The hardened stiffness parameter, k_3, and the amplitude of the fast oscillation, g, influence the dynamics of the VEH system. The width of the effective potential changes with increasing high-frequency (HF) amplitude, g. It implies that, via their cooperation, the system's performance can be controlled, which can improve the amount of vibration energy to be harvested.

The system's vibration is defined in terms of the deviation of the slow motion, h from the equilibrium point h^* by substituting $\Gamma = h - h^*$ in Eq. (24). Then

$$\begin{aligned} (\ddot{\Gamma} - \ddot{h}^*) &+ \lambda_1(\dot{\Gamma} - \dot{h}^*) + \beta(\dot{\Gamma} - \dot{h}^*)^3 + \lambda_2(\Gamma - h^*) \\ &+ \gamma_2(\Gamma - h^*)^3 = f\sin(\omega t). \end{aligned} \tag{27}$$

When the amplitude of the harmonic base displacement $Y \ll 1$, and the oscillation takes place around the equilibrium point ($h^* = 0$), then Eq. (27) becomes

$$\ddot{\Gamma} + \lambda_1\dot{\Gamma} + \beta(\dot{\Gamma} - \dot{h}^*)^3 + \lambda_2\Gamma + \gamma_2(\Gamma - h^*)^3 = f\sin(\omega t). \tag{28}$$

By neglecting the nonlinear term, we obtain a linear oscillator of the form

$$\ddot{\Gamma} + \lambda_1\dot{\Gamma} + \lambda_2\Gamma = f\sin(\omega t), \tag{29}$$

where $\omega_r = \sqrt{\lambda_2}$. Eq. (29) have a steady-state solution; $\Gamma = A_L\sin(\omega t)$. Therefore, the response amplitude A_L can be written as

$$\left.\begin{aligned} A_L &= \frac{f}{\sqrt{(\omega_r^2 - \omega^2)^2 + \lambda_1^2\omega^2}} \\ \theta &= -\tan^{-1}\left(\frac{\lambda_1\omega}{(\omega^2 - \omega_r^2)}\right) \end{aligned}\right\} \tag{30}$$

Finally, we can calculate the analytical response amplitude, Q from

$$Q = \frac{A_L}{f} = \frac{1}{\sqrt{(\omega_r^2 - \omega^2)^2 + \lambda_1^2\omega^2}}. \tag{31}$$

3.2. Numerical simulations

To validate the analytically computed response amplitude Q, we numerically integrate the nonlinear VEH oscillator (Eq. (6)) using the parameters settings in Fig. 3. This is achieved by first re-writing Eq. (6) as a set of coupled first-order Ordinary Differential Equations (ODEs) of the form

$$\begin{aligned} \frac{dz}{dt} &= \dot{z} \\ \frac{d\dot{z}}{dt} &= -\alpha\dot{z} - \beta\dot{z}^3 - \gamma z - \gamma_2 z^3 + f\sin(\omega t) + F\sin(\Omega t). \end{aligned} \tag{32}$$

Eq. (32) was integrated using the Fourth-Order Runge-Kutta scheme with a fixed step size $\Delta t = 0.001$, and the following parameters were set throughout the VR analysis; $k_1 = 5.0,\ c_1 = 0.20,\ Y = 0.05$ and $\Omega = 20\omega$, and the initial condition $[0, 1]$ was used. The response amplitude Q is computed from the Fourier spectrum of the time series of the output signal using the Fourier sine and cosine components B_S and B_C in the form

$$\left.\begin{aligned} Q &= \frac{\sqrt{B_S^2 + B_C^2}}{f} \\ \theta &= -\tan^{-1}\left(\frac{B_S}{B_C}\right), \end{aligned}\right\} \tag{33}$$

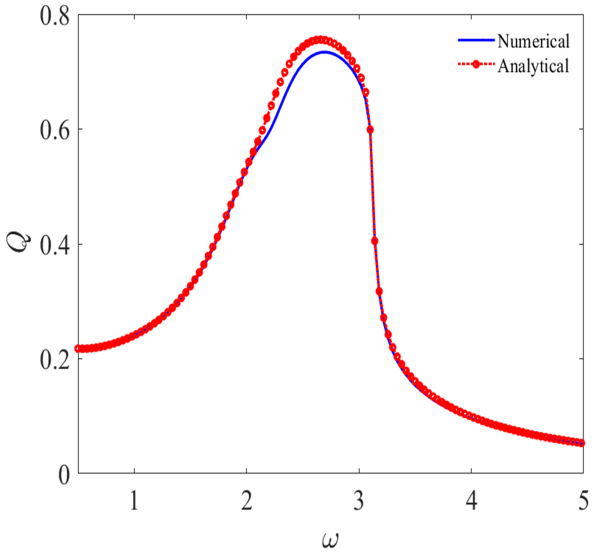

(a)

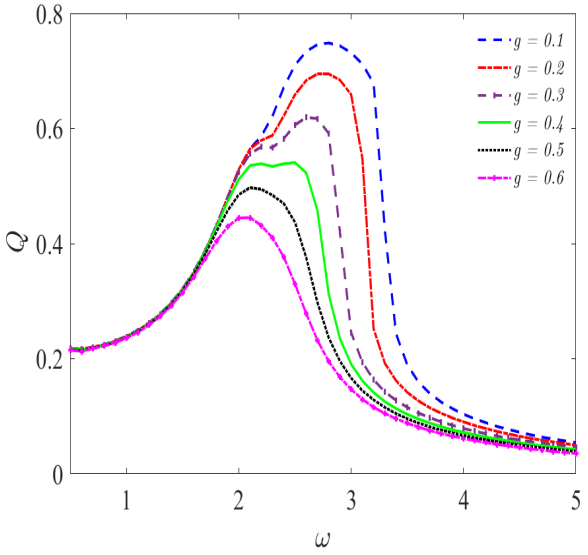

(b)

Figure 4: (a) Response plot Q as a function of the weak low-frequency, ω with $g = 0.1$. The continuous curve represents the numerical response plots, while the analytically calculated response amplitude Q from Eq. 31 is plotted with broken lines and markers, for $c_1 = 0.20$, $k_1 = 5.0$, $k_3 = 50$, $c_3 = 0.2, Y = 0.05$ and $\Omega = 20\omega$ and $m = 1.0$. (b) The dependence of Q on ω for six different values of g ($g = 0.1$, 0.2, 0.3, 0.4, 0.5 and 0.6), with other parameters of the VEH system fixed at $c_1 = 0.20$, $k_1 = 5.0$, $Y = 0.05$, $k_3 = 50$, $c_3 = 0.2$ and $\Omega = 20\omega$.

where,

$$\left.\begin{aligned} B_S &= \frac{2}{nT}\int_0^{nT} z(t)\sin\omega t\ dt, \\ B_C &= \frac{2}{nT}\int_0^{nT} z(t)\cos\omega t\ dt. \end{aligned}\right\} \tag{34}$$

$T = \frac{2\pi}{\omega}$ is the period of oscillation of the low-frequency input signal with $n = [1, 2, 3, \ldots]$ number of complete oscillations. To validate the analysis in Section 3, the analytically computed response amplitude Q obtained using Eq. (31) is compared with the numerical Q obtained directly from Eq. (33).

4. Results and Discussions

4.1. Occurrence of Vibrational Resonance

We now discuss the occurrence of vibrational resonance in the nonlinear VEH system. From in Eq. (31), the system's response amplitude is given by $Q = \frac{1}{\sqrt{S}}$, where $S = (\omega_r^2 - \omega^2)^2 + \lambda_1^2\omega^2$. In the linearized equation (Eq. (29)), the effective dissipation term λ_1 is a function of both the linear and nonlinear damping terms. We note that the highest power delivered by the system for any particular vibration energy harvester depends on the proper selection of load resistance regarding the effective dissipation [2, 12, 35]. Additionally, the occurrence of VR in any dynamical system suggests several control parameters and ascertains the availability of optimization variables [41, 55, 58].

To understand the effect of both the nonlinear damping and nonlinear stiffness on the resonance behaviour of the VEH system, we set $W = \omega_r - \omega$. Thus $S = W^2 - \lambda_1^2\omega^2$ suggests Q is maximum when S is minimum. This implies Q peaks at $W = 0$ ($\omega_r = \omega$), where $\omega_r = \sqrt{\lambda_2}$ and $\lambda_2 = \gamma_1 + 3\gamma_2\frac{F^2}{2\Omega^4}$. Since $\Omega \gg \omega$, resonance is expected to occur. Hence, $\omega_r^2 = \gamma_1 + 3\gamma_2(\frac{Y^2g^2}{2})$. This shows that ω_r is dependent on the values of k_1, k_3 and m through γ_1 and γ_2. Otherwise, if the oscillation amplitude is assumed to be small (e.g., $Y \ll 1$ and $g \geq Y$), then, $\omega_r = \sqrt{\gamma_1 + \gamma_2 g^2}$. This suggests three possible resonance cases.

Case I: Single-well condition, for $k_1 > 0$, $k_3 > 0$, when

$$k_1 \geq k_3 \tag{35}$$

Case II: Single-well-double-hump condition, for $k_1 > 0$, $k_3 < 0$, when

$$k_1 \gg k_3 \tag{36}$$

Case III: Double-well condition, for $k_1 < 0$, $k_3 > 0$, when

$$k_1 < k_3 \tag{37}$$

Here, the effective resonant frequency, ω_r^2, describes the potential structure of the system in relation to its resonant condition. These conditions correspond to three basic realizable potential shapes of any physical system with similar potential functions. Moreover, the forth condition ($k_1 \leq k_3 < 0$) is unrealistic because ω_r^2 is always greater

than zero. Eq. (26) enables us to analyze its occurrence with possibilities of multiple resonance peaks depending on the chosen parameter regime. The appearance of resonance peaks can be controlled by either modulating parameters of the fast periodic force (g or Ω) or the potential parameters (k_1 and k_3). From Eq. (35), Eq. (36), and Eq. (37), it can be seen that the system behaviour depends on the choice of k_3, which influences the resultant performance of the system at resonance.

The dependence of the response amplitude, Q, on the excitation low-frequency is shown in Fig. 4a for two reponse curves, obtained from the analytically computed response amplitude using Eq. (31) (red broken line with marker), and the numerically computed using Eq. (33) (blue continuous line). The analytical and numerical response curves are in good agreement. The deviation between the numerically and analytically computed response curves can be attributed to approximations in the derivation of the expression for the analytical Q. From the traditional theory of VR, one can examine the resonance behaviour of a dynamical system by changing the parameter ω, g or Ω. Therefore, the dependence of Q on ω for six different values of g ($g = 0.1,\ 0.2,\ 0.3,\ 0.4,\ 0.5$ and 0.6), with other parameters of the VEH system fixed at $c_1 = 0.20, c_3 = 0.2,\ k_1 = 5.0,\ Y = 0.05,\ k_3 = 50,$ and $\Omega = 20\omega$ is shown in Fig. 4b. It can be observed from the figure that increasing g reduces the response amplitude. This is because the resonant frequency is independent of ω, and the mechanism of resonance is the minimization of the function, $S = (\omega_r^2 - \omega^2)^2 + \lambda_1^2\omega^2$, which remains constant even when ω is changed. The dependence of the system's response Q on low-frequency (LF) parameter, ω can also be controlled by the nonlinear parameters of the system, as shown in Fig. 5.

To gain further insight into the contributions of nonlinearities on the response of the VEH system, we present the dependence of response amplitude, Q, on the low-frequency, ω for four values of the cubic stiffness, $k_3 = [5,\ 50,\ 110,\ 220]$ with $k_1 = 5.0,\ g = 0.10,\ c_1 = 0.2,\ c_3 = 0.2, Y = 0.05,$ and $\Omega = 20\omega$ in Fig. 5a. The cubic stiffness parameter, k_3 tuned the resonance state of the system with an obvious reduction in response amplitude Q, as the nonlinear stiffness parameter, k_3 is increased from 0 to 220. Also, increasing k_3 shifts the peak points of the response curve to the right and increases the bandwidth, which can aid system performance. This observation is consistent with Literature, and nonlinear hardening spring (i.e., $k_3 > 0$) increases the resonant frequency of a vibration isolation system by shifting the peak magnitude to the right [14, 12]. Consequently, this suggests the harvesting of energy over an extended bandwidth by the VEH system. On the other hand, Fig. 5b depicts the variation of Q with ω for four different values of the cubic damping parameter, $c_3 = [0.0, 0.2,\ 0.3,\ 0.6]$, with $c_1 = 0.2,\ g = 0.1,\ Y = 0.05,\ k_1 = 5.0,\ k_3 = 50$ and $\Omega = 20\omega$. Increasing c_3, the cubic damping parameter suppresses the response amplitude, Q and lowers the system's resonant frequency.

The resonance state of the VEH system is highly dependent on the imposed nonlinearities. Consider the system's response at resonance, the response amplitude, Q becomes maximum whenever the resonant frequency, ω_r matches with the vibration frequency, ω of the external excitation ($\omega_r^2 = \omega^2$). Therefore, from Eq. 31, Q depends on the damping terms through λ_1. Thus, a further increase in the value of c_3 leads to the condition, $\omega_r > \omega$, and the resonance peaks disappear. The effect of damping on the dynamical response of a system has been well-studied, and similar effects were reported [20, 33].

4.2. Controlling VR with VEH system's parameters

We only considered the first resonance condition ($k_1 > 0$ and $k_3 > 0$) for the occurrence of the VR phenomenon in this paper. Firstly, we examined the effect of modulating the system's parameters on the VR phenomenon. Fig. 6a and Fig. 6b show the variation of the response amplitude Q on the high-frequency signal amplitude g for different values of the linear damping and the linear stiffness parameters, respectively. Both figures exhibit two resonant peaks for the parameter values considered. In Fig. 6a, response plots for six different values of the linear damping $c_1 = [0.2,\ 0.3,\ 0.4,\ 0.5,\ 0.6,\ 0.7]$, were superimposed. There is a marked decrease in the system's response as c_1 increases. As observed, the effect of the linear damping, on the response amplitude, Q, of the VEH system, is to reduce Q as g varies. Fig. 6b shows the dependence of Q on g for $k_1 = [2.5,\ 3.0,\ 3.5,\ 4.0,\ 4.5,\ 5.0]$, with $k_3 = 50,\ c_1 = 0.2,\ c_3 = 0.2,\ Y = 0.05\ \omega = 0.3$ and $\Omega = 20\omega$. Increasing the strength of the linear stiffness, k_1, decreases the response amplitude Q of the system and shifts the response peaks to the left. Increase in magnitudes of both the linear damping and the linear stiffness parameters, c_1 and k_1, respectively, lowers the value of Q. In addition, adjusting c_1 shifts the response curves to the right, contrary to the effects of modulating k_1. The effect of the nonlinear damping on the dynamical response of the VEH system is considered in Fig. 7. In Fig. 7a, three distinct VR peaks were observed with $c_3 = 0.0$, in the range $0 < g < 3$, with their magnitudes increasing as g varies within the range. On activating the nonlinear damping, $c_3 = 0.2$, the VR peaks reduced and their magnitudes decrease monotonically with increasing g. The peaks are reduced to single resonance curves in Fig. 7b, Fig. 7c and Fig. 7d, when $c_3 = 0.30,\ c_3 = 0.40$ and $c_3 = 0.60$, respectively. Due to the high value of c_3, the disappearance of the multiple VR curves are pronounced in Fig. 7c and Fig. 7d, showing the possibility of suppressing VR, when the nonlinear damping is further increased. Consequently, when c_3 surpasses specific critical levels, resonance vanishes, and the system harvests no significant energy.

Next, we examined the effect of nonlinear stiffness, k_3, on the response amplitude of the VEH system in Fig. 8a-d. Increasing k_3 enhances the system's response Q, with

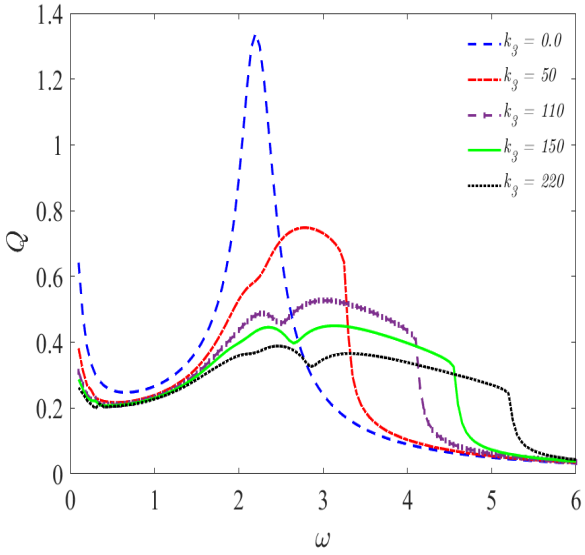

(a)

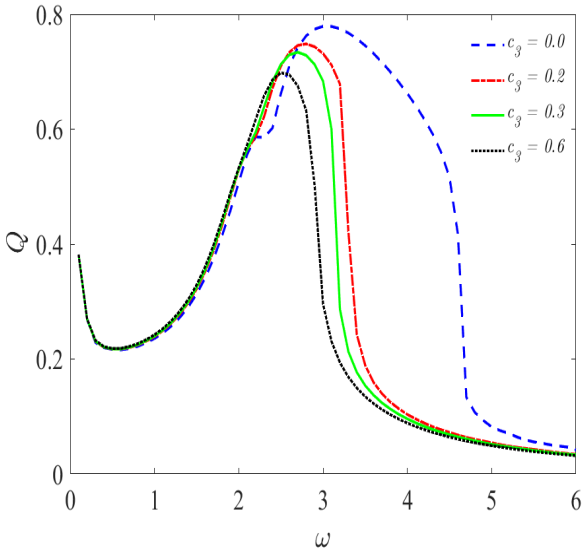

(b)

Figure 5: The dependence of response amplitude, Q on the weak oscillation frequency, ω for: (a) five different values of the nonlinear stiffness, $k_3(k_3 = 0,\ 50,\ 110,\ 150$ and $220)$ with $k_1 = 5.0,\ g = 0.10,\ c_3 = 0.2, Y = 0.05,$ and $\Omega = 20\omega$; (b) for four different values of the nonlinear damping, $c_3(c_3 = 0.0,\ 0.20,\ 0.30,$ and $0.60)$ with $c_1 = 0.2,\ g = 0.1,\ Y = 0.05,\ k_3 = 50,$ and $\Omega = 20\omega$.

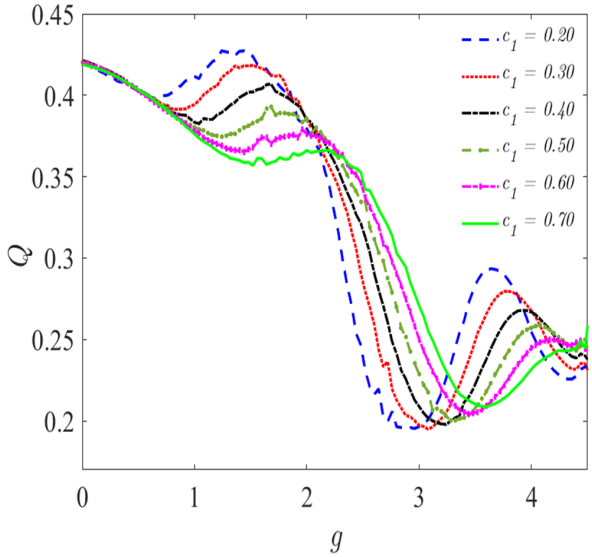

(a)

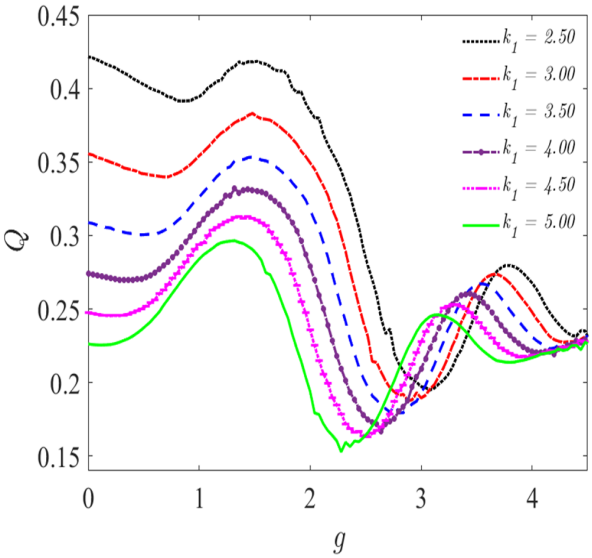

(b)

Figure 6: (a) Dependence of Q on the amplitude of the fast oscillation g, with varying linear damping c_1 when other parameters of the VEH system are fixed at $k_1 = 5.0,\ k_3 = 50,\ c_3 = 0.2, Y = 0.05\ \omega = 0.3$ and $\Omega = 20\omega$; (b) The dependence of Q on g for $k_1 = 2.5,\ 3.0,\ 3.5,\ 4.0, 4.5$ and 5.0 with $k_3 = 50,\ c_1 = 0.2,\ c_3 = 0.2,\ Y = 0.05\ \omega = 0.3$ and $\Omega = 20\omega$.

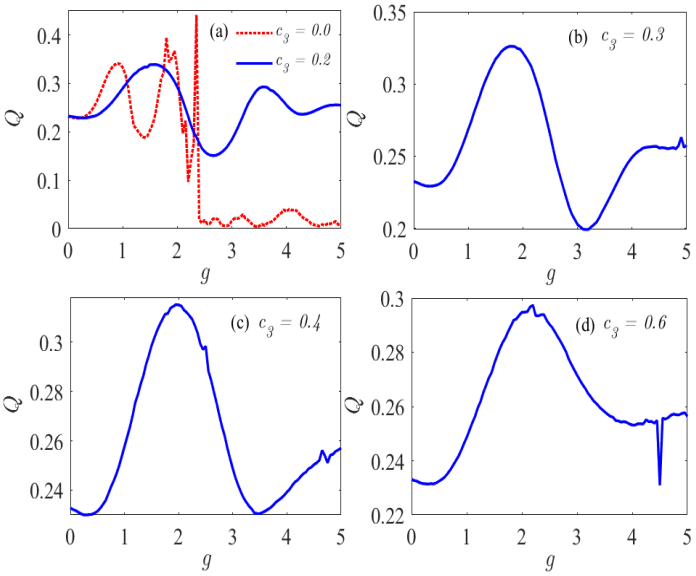

Figure 7: Dependence of Q on g for (a) $c_3 = 0.0$ and 0.20, (b) $c_3 = 0.30$, (c) $c_3 = 0.40$ and (d) $c_3 = 0.60$ with other parameters of the VEH system fixed at $c_1 = 0.20$, $k_1 = 5$, $Y = 0.05$, $k_3 = 50$, $\omega = 0.3$ and $\Omega = 20\omega$.

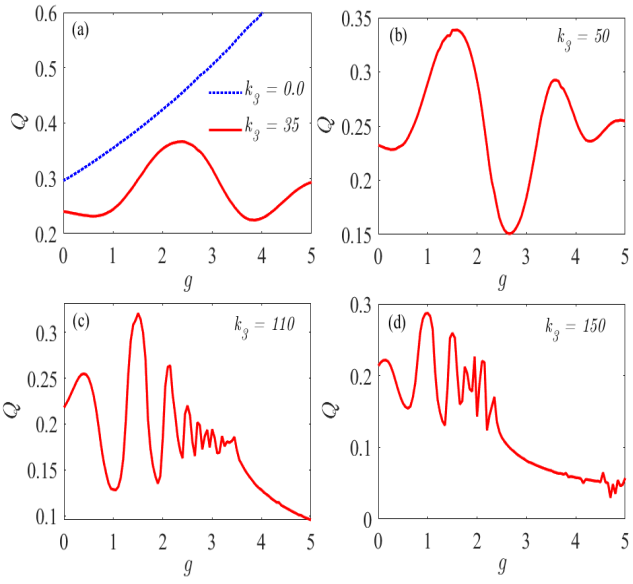

Figure 8: Response plot Q against g the amplitude of the fast oscillation with, (a) nonlinear stiffness parameter $k_3 = 0.0$ and $k_3 = 35$, (b) $k_3 = 50$, (c) $k_3 = 110$ and (d) $k_3 = 150$, while other parameters of the system are $c_1 = 0.20$, $k_1 = 5$, $Y = 0.05$, $c_3 = 0.2$, $\omega = 0.3$ and $\Omega = 20\omega$.

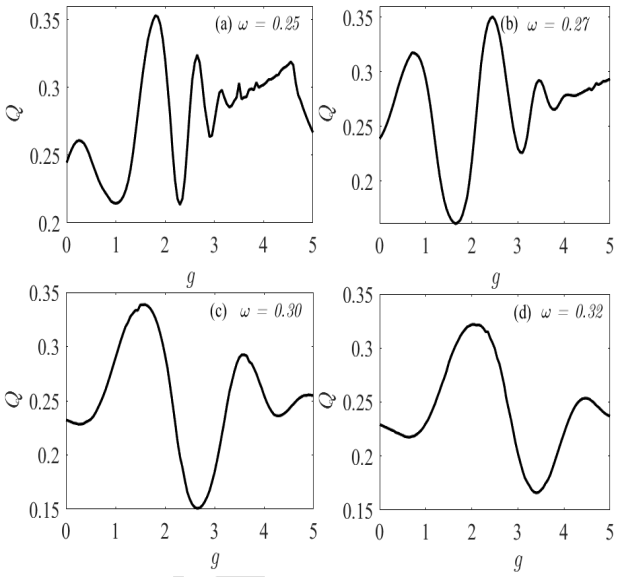

Figure 9: Dependence of Q on g for different values of weak frequency (a) $\omega = 0.25$, (b) $\omega = 0.27$, (c) $\omega = 0.30$ and (d) $\omega = 0.32$ with other parameters of the VEH system fixed at $c_1 = 0.20$, $k_1 = 5$, $Y = 0.05$, $c_3 = 0.20$, $k_3 = 70$ and $\Omega = 20\omega$.

the emergence of more VR curves, highlighting the cooperation of amplitude of the fast excitation g and the hardened stiffness, k_3. Consequently, multiple resonance peaks were created. The occurrence of VR in the first figure (Fig. 8a) without activating the nonlinear stiffness, $k_3 = 0$, appears impossible, for the considered range of g ($g \in [0, 5]$). However, the increased value of k_3 in Fig. 8a, when $k = 35$, ascertained the occurrence of VR. With $k_3 = 50$, in Fig. 8b, two significant VR peaks were observed. Moreover, the emergence of multiple VR peaks in Fig. 8c and Fig. 8d, with $k_3 = 110$ and $k_3 = 150$, respectively, appeared in the range $0 < g \leq 3$. We fixed the values of other parameters of the VEH system and adjusted the excitation frequency, ω, to examine its significant impact on the system's dynamics. Figures 9a-d show the dependence of Q on g for four different values of the excitation ($\omega = [0.25, 0.27, 0.30, 0.32]$), with $c_1 = 0.20$, $k_1 = 5$, $Y = 0.05$, $c_3 = 0.20$, $k_3 = 50$ and $\Omega = 20\omega$. The figures demonstrate that varying ω has an influence on the system's dynamics, similar to c_3; they reduce the system's response amplitude and ultimately cause VR to disappear [30]. In Fig. 9, multiple resonance peaks, which decrease, both in magnitude and numbers, as ω increase from 0.27 to 0.32, were observed. Therefore, increasing frequency, ω will reduces the response amplitude Q due to $\omega_r \neq \omega$, implying no resonance. A similar effect has been reported in the literature. The majority of earlier findings established that when either the frequency or the damping rises above certain critical values, the response amplitude Q of dynamical systems decreases and may even vanish entirely [33, 30].

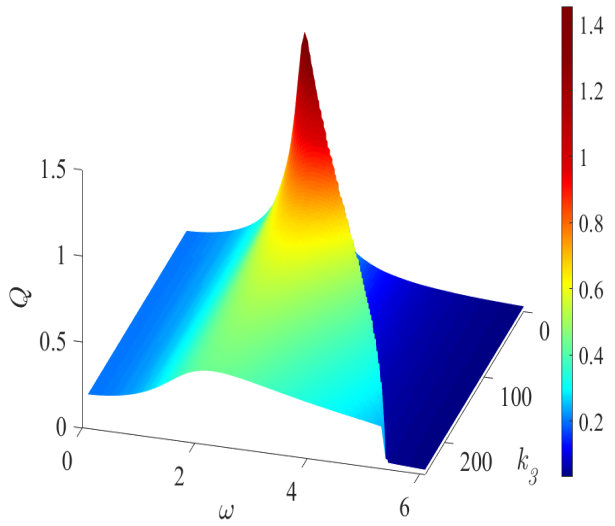

(a)

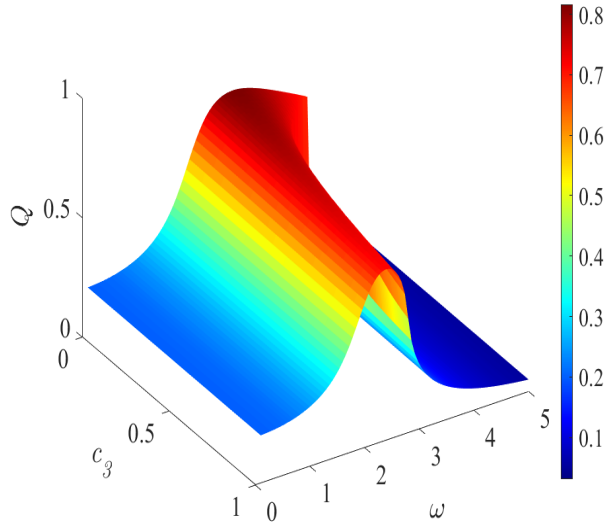

(b)

Figure 10: Three-dimensional plot showing the dependence of Q on (a) the hardening stiffness, k_3, with varying LF component ω, when other parameters of the VEH system are fixed at $k_1 = 5.0$, $k_3 = 50$, $c_3 = 0.2$, $Y = 0.05, g = 0.1$, and $\Omega = 20\omega$; (b) the nonlinear damping parameter, c_3, with varying LF component ω, when other parameters of the VEH system are fixed at $k_1 = 5.0$, $k_3 = 50$, $Y = 0.05$, $g = 0.1$ and $\Omega = 20\omega$.

To illuminate broader feature of the response in the considered parameter regime, we explored three-dimensional (3D) plots, shown in Fig. 10 and Fig. 11a. The dependence of Q on the hardening stiffness, k_3, with varying LF component ω is shown in Fig. 10a, when other parameters of the system are fixed at, $c_1 = 0.20$, $k_1 = 5.0$, $c_3 = 0.2$, $Y = 0.05$, $g = 0.1$ and $\Omega = 20\omega$. It is evident from the figure (Fig.10a) that a single resonance appears for the considered values of the hardening stiffness ($k_3 \in [0, 250]$), forming a ridge-shaped elevation with the peak in red. Figure 10b, presents the dependence of the system's response on the nonlinear damping parameter, c_3, with varying LF component ω, when other parameters are fixed at, $k_1 = 5.0$, $k_3 = 50$, $Y = 0.05$, $g = 0.1$ and $\Omega = 20\omega$. The red-coloured hill corresponds to high response amplitude Q values, which stretch along c_3 values. This is more pronounced for lower values of the nonlinear damping, c_3. Both plots, Fig. 10a and Fig. 10b, confirmed the evidence for just a single resonance curve, which amplitude can be controlled by the modulation of the nonlinear parameters, k_3 and c_3, respectively. Moreover, the 3D-plots in Fig. 10a and Fig. 10b, are in agreement with Fig. 5a and Fig. 5b, respectively. Interestingly, the figures confirmed our prediction of resonance conditions (i.e. Eq. (35)).

To corroborate our results and discussions on VR occurrence, and validate that the system's performance can be optimized using VR approach, the dependence of Q on g and ω is shown in Fig. 11a. Figure 11a shows 3D-plot of the dependence of the system's response amplitude, Q on the amplitude of the fast oscillation, g and the LF component, ω, when other parameters of the VEH system are fixed at $k_1 = 5.0$, $k_3 = 50$, $c_3 = 0.2$, $Y = 0.05$ and $\Omega = 20\omega$. The hill-shaped figure represents the VR curve, with its peak in red.

The enhancement regime is more pronounced when $g < 0.5$. The blue plains are indication of no enhancement. It is clear from the figure (Fig.11a) that lower values of g is required to enhance the system's performance. To broadly examine the features of the system's response and the significance of nonlinearities on the system, we present the dependence of the response amplitude Q on the nonlinear damping parameter c_3 with and without the activation of the fast oscillation in Fig11b. The plots confirmed the optimization of the systems performance with a low value of g and the nonlinear damping range $0 < c_3 < 0.6$, which supports maximum energy conversion. The figure shows the maximum response amplitude Q_{max} occurs at $c_3 = 0.2$ for both cases; $g = 0.00$ and $g = 0.10$. These values ($g = 0.1$ and $c_3 = 0.20$) were used for further analyses and for the estimation of the average power harvested by the system.

5. Average Power absorbed by the system

In this section, we analyzed the effect of nonlinearities on the resultant energy harvested by the nonlinear vibration energy harvester described in Eq. 6. The occurrence

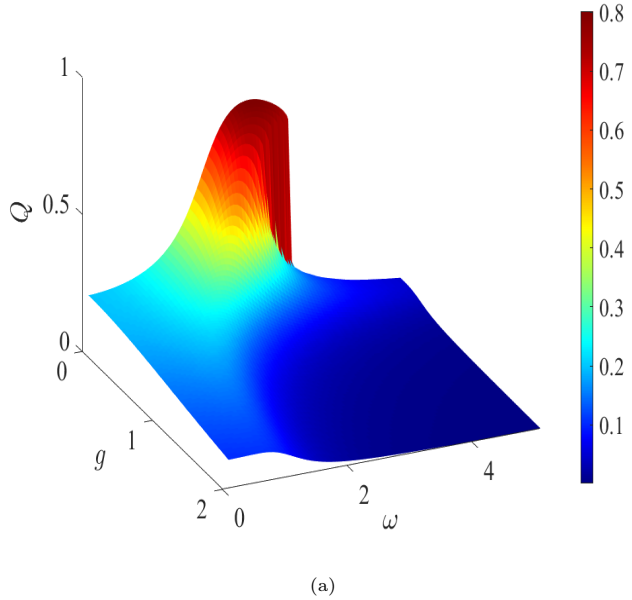

(a)

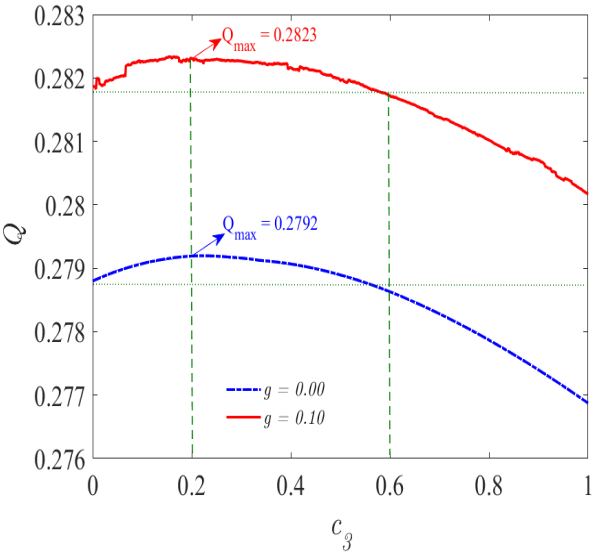

(b)

Figure 11: Three-dimensional plot showing the dependence of Q on the amplitude of the fast oscillation, g, with varying LF component ω. Other parameters of the system were fixed at, $c_1 = 0.20$, $k_1 = 5.0$, $c_3 = 0.2$, $Y = 0.05$, $k_3 = 50$ and $\Omega = 20\omega$. (b) The dependence of the system's response Q on the nonlinear damping parameter c_3, with and without the activation of the fast oscillation, when other parameters are fixed at $k_1 = 5.0$, $k_3 = 5$, $Y = 0.05$, $\omega = 0.3$ and $\Omega = 20\omega$.

of resonance generally describes any response amplification of a system where improvement occurs through the adjustment of any system parameter, not necessarily frequency [30, 49, 58]. Also, under resonance conditions the system must have acquires considerable energy resulting in an amplified response. So we related our previous discussion on the analysis of VR to the amount of energy harvested by the VEH system. We showed the possibility of optimizing the system's performance. We estimated the amount of energy harvested numerically, and established that the parameter values maximize the system response in average electrical power. In any event, the instantaneous power absorbed by electromagnetic damper is dependent on the instantaneous damping force and relative displacement of the damper [12, 14, 56].

Next, we analyse the resultant average power generated by expressing P_{av} as

$$P_{av} = \frac{1}{T}\int_0^T (c_3\dot{z}^3)\dot{z}dt, \tag{38}$$

such that for the low frequency harmonic oscillation with displacement $z(t) = Z\sin(\omega t)$, where Z is the amplitude of the solution to Eq. (1). Consequently, the magnitude of the average power generated by the system can then be obtained as defined in [14] from

$$P_{av} = \frac{3}{8}c_3\omega^4 Z^4. \tag{39}$$

It should be noted from Fig. 1 that energy is lost from the system through c_1, while from Eq. (39), the cubic damping c_3 gainfully contributes to the total amount of energy harvested by the system (Eq. 39). More so, the system's dynamics, particularly the response amplitude is dependent on the harmonic excitation frequency, ω, and the nonlinear parameters (c_3 and k_3). Hence, the impact of the nonlinear parameters on the amount of harvested energy is substantial. In Fig. 12a, the variation of average power, P_{av} with oscillation frequency, ω is shown for different values of the amplitude of the fast vibration, $g = [0.1, 0.2, 0.3, 0.4]$, with other parameters of the system fixed at $k_3 = 50$, $Y = 0.05$, $c_1 = 0.20$, $c_3 = 0.20$, $k_1 = 5.0$ and $\Omega = 20\omega$. Increasing g from g decreases the average power, P_{av}. The effect of modulating cubic stiffness on the average power absorbed, is described in Fig. 12b. The system can absorb more energy as k_3 increases. The impact of hardening stiffness, k_3, on the the average power is clear, it extends the operational bandwidth of the VEH system by increasing the resonance frequency, and improve the amount of energy harvested. Therefore, the system's adequate performance depends on the appropriate choice of k_3, as obviously shown in Fig. 12b.

It is worth mentioning that the power is absorbed at resonance ($\omega_r = \omega$). With a fixed value of the LF component ($\omega = 0.30$), it is expected that P_{av} increases with increasing g or c_3, due to its direct dependence on c_3 and Z from Eq. (39). To analyse the effect of c_3 on P_{av}, Fig.

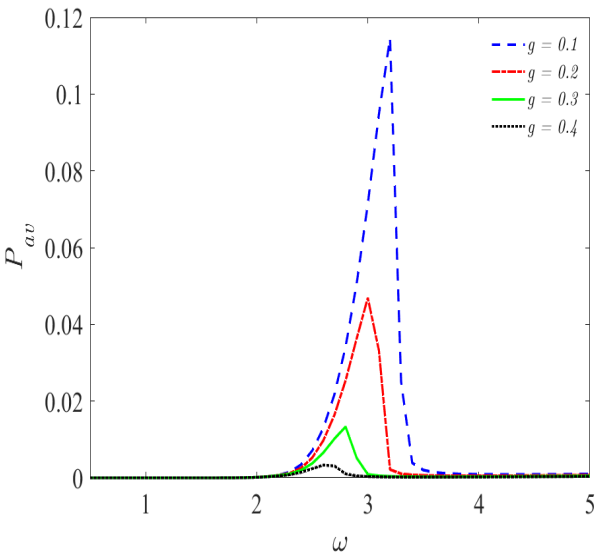

(a)

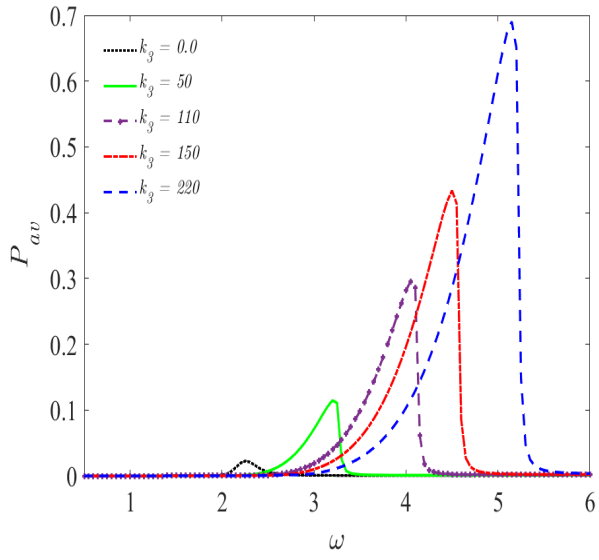

(b)

Figure 12: (a) The variation of average power P_{av} with oscillation frequency, ω for different values of; (a) the amplitude of the fast vibration, $g = [0.10, 0.20, 0.30, 0.4]$, with other parameters of the system fixed at $k_3 = 50$, $Y = 0.05$, $c_1 = 0.20$, $c_3 = 0.20$, $k_1 = 5.0$ and $\Omega = 20\omega$; (b) the nonlinear stiffness, $k_3 = [0, 50, 110, 150, 220]$, with other parameters fixed at $k_1 = 5.0$, $g = 0.10$, $c_3 = 0.2, Y = 0.05$, and $\Omega = 20\omega$

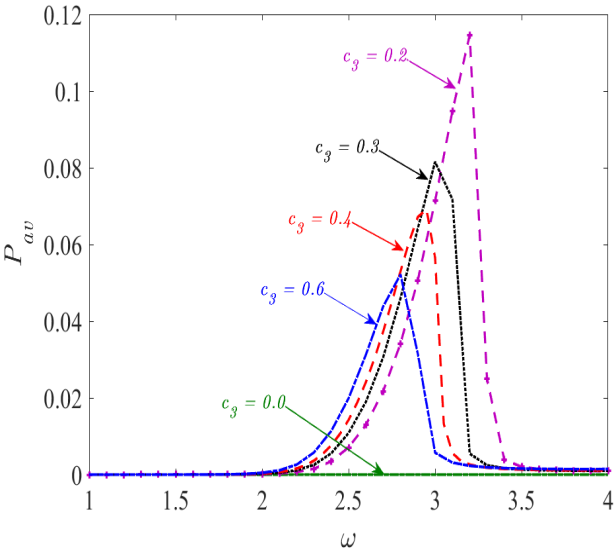

(a)

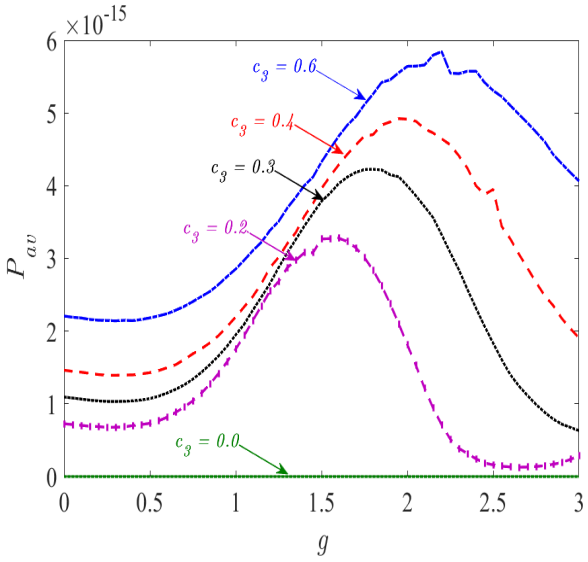

(b)

Figure 13: (a) The variation of average power P_{av} with frequency, ω for different values of nonlinear damping, c_3 ($c_3 = [0.0, 0.2, 0.4, 0.6]$), with other parameters fixed at $k_1 = 5.0, k_3 = 50$, $g = 0.10$, $c_3 = 0.2, Y = 0.05$, and $\Omega = 20\omega$. (b) Dependence of the average power, P_{av} on the amplitude of the fast oscillation g, for different values of nonlinear damping, c_3 ($c_3 = [0.0, 0.2, 0.4, 0.6]$), with other parameters fixed at $k_1 = 5.0$, $\omega = 0.3$, $c_3 = 0.2, k_3 = 50, Y = 0.05$, and $\Omega = 20\omega$.

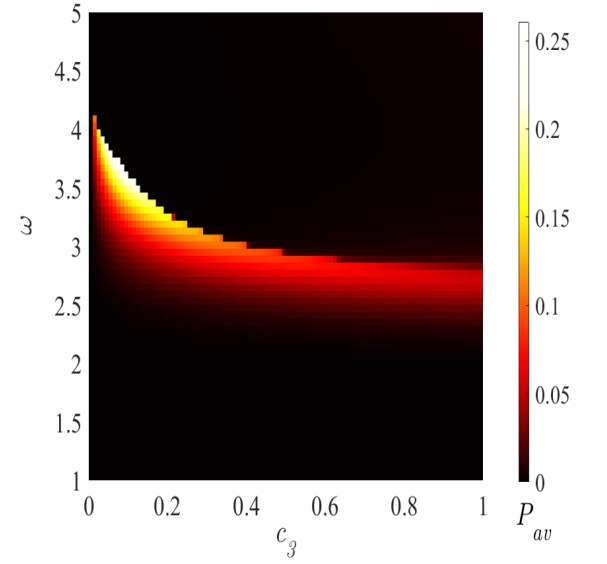

(a)

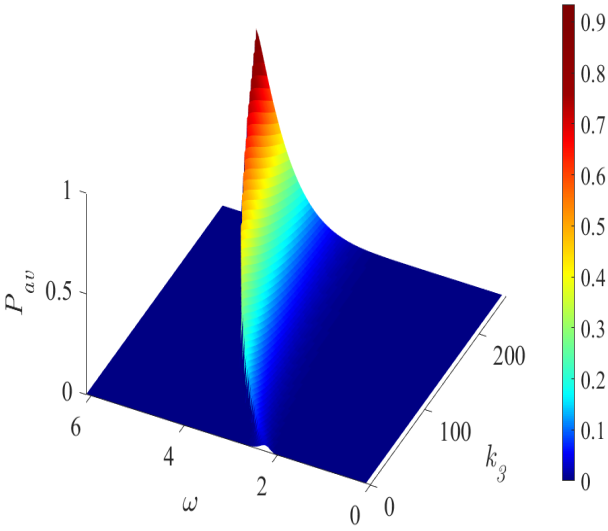

(b)

Figure 14: Three-dimensional plot showing the dependence of the average power, P_{av} on (a) the nonlinear damping parameter, c_3, with varying LF component ω, when other parameters of the VEH system are fixed at, $k_1 = 5.0$, $k_3 = 50$, $Y = 0.05$, $g = 0.1$ and $\Omega = 20\omega$; (b) the hardening stiffness, k_3, with varying LF component ω. Other parameters of the system were fixed at, $c_1 = 0.20$, $k_1 = 5.0$, $c_3 = 0.2$, $Y = 0.05$, $g = 0.1$ and $\Omega = 20\omega$.

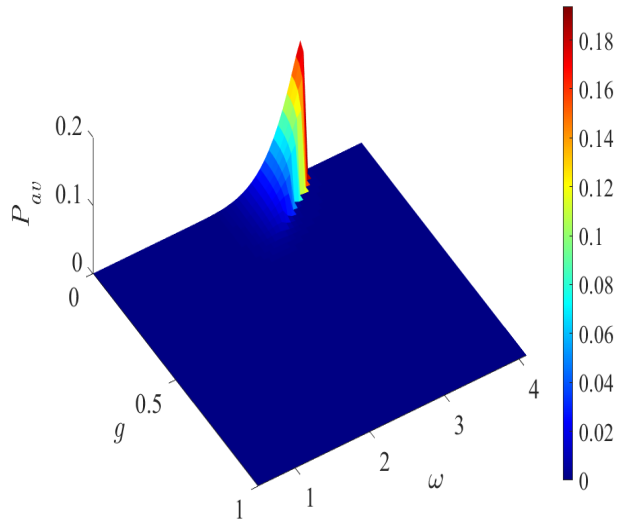

(a)

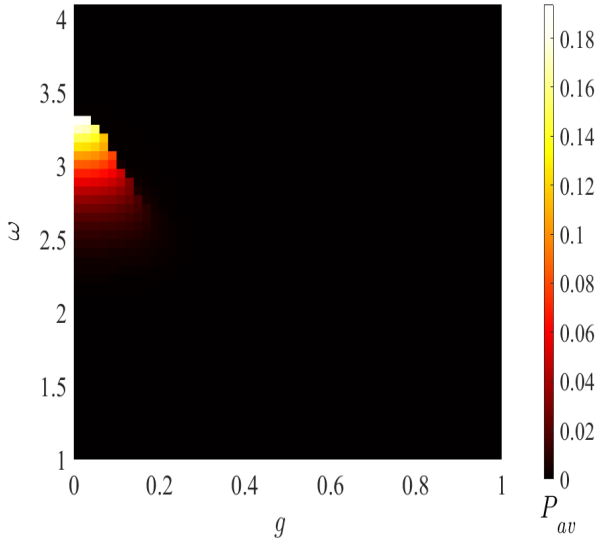

(b)

Figure 15: Three-dimensional plot showing the dependence of the average power, P_{av} on the amplitude of the fast oscillation g, with varying LF component ω, when other parameters of the VEH system are fixed at $k_1 = 5.0$, $k_3 = 50$, $c_3 = 0.2, Y = 0.05$ and $\Omega = 20\omega$. (b) A two-parameter space plot of Fig. 15a.

13a depicts the variation of average power, P_{av} with frequency, ω for different values of the cubic damping c_3. It is worth noting that the effect of increasing c_3 on P_{av}, as shown in the figure, is similar to the significant impact of g on the absorbed power in Fig. 12a. Dependence of the average power, P_{av} on the amplitude of the fast oscillation g, for different values of the nonlinear damping, c_3 ($c_3 = [0.0, 0.2, 0.4, 0.6]$), with other parameters fixed at $k_1 = 5.0$, $\omega = 0.3$, $c_3 = 0.2, Y = 0.05$, and $\Omega = 20\omega$, is shown in Fig. 13b. Despite the low magnitude, P_{av} increases with increasing c_3 and g. This is as expected from Eq. (39), with fixed value of ω. On the other hand, with varying values of ω, it is essential to consider the response behaviour and the amount of energy generated by the VEH system, with respect to the natural resonant frequency of the system. This is because the resonant frequency, fundamentally defines the dynamical behaviour of the system, especially at resonance. Recently, it was reported that the behaviour of a dynamical system is a function of its natural frequency, particularly, the response dynamics [57, 58].

From the response curves, Fig. 5b and Fig. 7, increasing the nonlinear damping, c_3, reduces the resonant frequency (frequency of interest) and the response amplitude, respectively, which as well, decreases the average power absorbed by of the VEH system (Fig. 13a). This therefore suggests a range of values for c_3, for which the performance of the nonlinear energy harvester can be optimised. Consequently, we presents a three-dimensional plot showing the dependence of the average power, P_{av} on the nonlinear damping parameter, c_3, with varying LF component ω, when other parameters of the VEH system are fixed at, $k_1 = 5.0$, $k_3 = 50$, $Y = 0.05$, $g = 0.1$ and $\Omega = 20\omega$, in Fig. 14a. To illuminate broader features of the nonlinear damping on the average power absorbed by the system, we explore the figure in a two-parameter space, showing the dependence of P_{av} on the parameters, ω and c_3. The average power absorbed increases with lightness/brightness (see the colour bar), and the peak is white. Clearly, P_{av} is maximum at a low value of the nonlinear damping, in the range, $0 < c_3 \leq 0.2$. In Fig. 14b, we presents a 3D-plot of the dependence of P_{av} on the hardening stiffness, k_3, with varying LF component ω. Other parameters of the system were fixed at, $c_1 = 0.20$, $k_1 = 5.0$, $c_3 = 0.2$, $Y = 0.05$, $g = 0.1$ and $\Omega = 20\omega$. It is evident from the figure (Fig. 14b) that P_{av} increases with increasing hardening stiffness, k_3.

To corroborate our results and discussions on VR occurrence, and validate that the average power the system absorbs depends on the imposed nonlinearities, we present three-dimensional plot of the dependence of P_{av} on g and ω in Fig. 15. From the figure, particularly, in Fig. 15a, it was observed that the system can harvest appreciable amount of energy. Moreover, it is clear from Fig. 15b, that the performance of the VEH system can only be optimised with lower values of g ($g \leq 0.1$). It is worth mentioning that practical VEH systems are typically constrained in their relative displacement, Z, imposing optimization

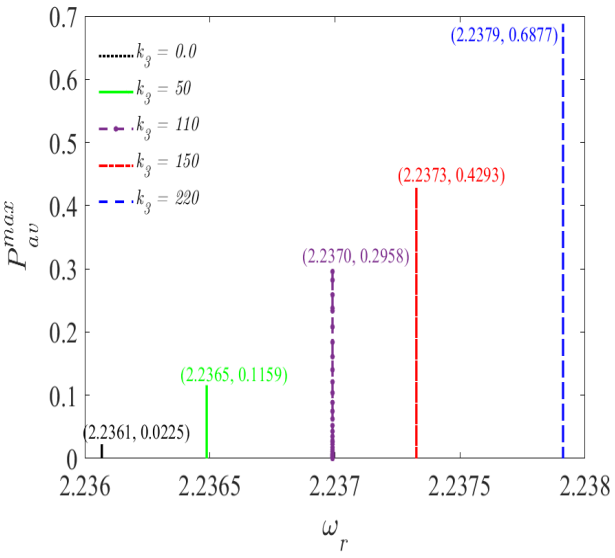

Figure 16: Dependence of the maximum average power P_{av}^{max} on the effective resonant frequency ω_r, showing the effect of varying the nonlinear stiffness parameter k_3 on ω_r when other parameters are fixed at $c_1 = 0.20$, $k_1 = 5.0$, $c_3 = 0.2$, $Y = 0.05$, $g = 0.10$ and $\Omega = 20\omega$.

challenges. The fact that the system's response, Q, which is proportional to Z, is dependent on g for VR occurrence, shows that our results and discussions are substantial for the optimization of the VEH system.

To assess the impact of the nonlinear stiffness parameter and the resonant frequency, particularly on the amount of energy harvested by system (6), we examined the change in the effective resonant frequency and quantify the average power harvested by system. This is shown in Fig. 16. It can be seen from Fig. 12b that P_{av} increases with increasing k_3. More so, the optimal value of the average power (P_{av}^{max}) harvested by the VEH system is observed at different excitation frequency. This implies that the energy conversion that takes place whenever $\omega_r = \omega$ can be controlled with k_3 as shown in Fig. 16. Therefore, with the appropriate choice of the nonlinear stiffness parameter k_3, the system's performance can be improved. For instance, the corresponding optimal values (ω_r, P_{av}^{max}) to the curves in Fig. 12b are $(2.2361, 0.0225), (2.2365, 0.1159), (2.2370, 0.2958), (2.2373, 0.4293), (2.2379, 0.6877)$ for $k_3 = [0.0, 50, 110, 150, 220]$, respectively. The optimization values of the system's parameters are summarised in Table 1.

6. Conclusion

In this study, the effect of nonlinear parameters, on the energy harvested by a nonlinear VEH system, was investigated. We examined the influence of the nonlinear damping and stiffness parameters on the system's resonance state for the single-well potential structure. We quanti-

Table 1: Summarised optimal values of the system's parameters while other parameters are fixed at $m = 1.0, c_1 = 0.20, Y = 0.05, g = 0.10$ $\omega = 0.3$ and $\Omega = 20\omega$.

Parameter	Range	Optimal value	P_{av}^{max}
c_3	$0 < c_3 \leq 0.60$	0.20	0.1146
k_3	$5.0 \leq k_3 \leq 220$	220	0.6877

fied the possible amount of energy harvested in terms of average power absorbed by the vibratory system using a dual-periodic forcing mode of vibrations (one with high-frequency, Ω, and the other with low-frequency, ω). VR was characterized by the analytical and numerical computation of response amplitude. To demonstrate the concordance between our theoretical and numerical results, the response curves for the variation and response amplitude, Q with relevant system parameters were compared.

Our research demonstrated that the VEH system produced more energy when the nonlinear parameters are tuned. The presence of nonlinear stiffness, k_3, extended the system's bandwidth. We also identified a permitted value of the low frequency forcing ω, for which the system's average power gain can be enhanced with low values of k_3. Therefore, P_{av} is optimized with c_3. Also, we demonstrated that the nonlinear VEH may harvest significant power at resonance, through the collaboration of ω and k_3, in the appropriate choice of the nonlinear damping, c_3. The calculated average power absorbed, P_{av}, and the system's response, Q, for various system parameter values produced the regimes for enhanced energy harvesting. In most mechanical and electromechanical systems, vibrational energy requires matching the system's resonant frequency to the oscillation frequency, hence, we demonstrated that the system's resonance frequency is a crucial factor in characterizing the response of the VEH system and identifying the proper parameter selection to improve the system's efficiency.

Our findings would benefit a VEH design with severe nonlinearities and enclosure-based physical limitations. In terms of application, we propose an electromagnetic damper made of permanent magnets, wire coils, and artificially constructed 3D-printed structures, or an electromechanical device with a nonlinear electrical load be used to achieve the nonlinear damping characteristic of a VEH system.

References

[1] M. Coccolo, G. Litak, J. M. Seoane, M. A. F. Sanjuán, Energy harvesting enhancement by vibrational resonance, International Journal of Bifurcation and Chaos 24 (2014) 1430019.

[2] D. Su, K. Nakano, R. Zheng, M. P. Cartmell, On electrical optimisation using a duffing-type vibrational energy harvester, Proceedings of the Institution of Mechanical Engineers, Part C: Journal of Mechanical Engineering Science 229 (2015) 3308–3319.

[3] Z. Yang, Y. Zhu, J. Zu, Theoretical and experimental investigation of a nonlinear compressive-mode energy harvester with high power output under weak excitations, Smart Materials and Structures 24 (2015) 025028.

[4] B. Yan, S. Zhou, G. Litak, Nonlinear analysis of the tristable energy harvester with a resonant circuit for performance enhancement, International Journal of Bifurcation and Chaos 28 (2018) 1850092.

[5] U. Diala, Y. Zhu, R. Gunawardena, Investigative study of the effect of damping and stiffness nonlinearities on an electromagnetic energy harvester at low-frequency excitations, Machines 12 (2024) 30.

[6] N. G. Stephen, On energy harvesting from ambient vibration, Journal of sound and vibration 293 (2006) 409–425.

[7] T. Yang, S. Zhou, S. Fang, W. Qin, D. J. Inman, Nonlinear vibration energy harvesting and vibration suppression technologies: Designs, analysis, and applications, Applied Physics Reviews 8 (2021) 031317.

[8] C. Wei, K. Zhang, C. Hu, Y. Wang, H. Taghavifar, X. Jing, A tunable nonlinear vibrational energy harvesting system with scissor-like structure, Mechanical Systems and Signal Processing 125 (2019) 202–214.

[9] B. Seyed-Aghazadeh, H. Samandari, S. Dulac, Flow-induced vibration of inherently nonlinear structures with applications in energy harvesting, Physics of Fluids 32 (2020) 071701..

[10] M. Hendijanizadeh, S. J. Elliott, M. Ghandchi-Tehrani, Extending the dynamic range of an energy harvester with a variable load resistance, Journal of Intelligent Material Systems and Structures 28 (2017) 2996–3005.

[11] M. G. Tehrani, S. J. Elliott, Extending the dynamic range of an energy harvester using nonlinear damping, Journal of Sound and Vibration 333 (2014) 623–629.

[12] R. Ramlan, M. Brennan, B. Mace, I. Kovacic, Potential benefits of a non-linear stiffness in an energy harvesting device, Nonlinear dynamics 59 (2010) 545–558.

[13] P. Green, K. Worden, K. Atallah, N. Sims, The benefits of duffing-type nonlinearities and electrical optimisation of a mono-stable energy harvester under white gaussian excitations, Journal of sound and vibration 331 (2012) 4504–4517.

[14] U. Diala, R. Gunawardena, Y. Zhu, Z.-Q. Lang, Nonlinear design and optimisation of a vibration energy harvester, in: 2018 UKACC 12th international conference on control (CONTROL), IEEE, 2018, pp. 180–185.

[15] Z.-J. Liao, Y.-H. Sun, Y. Liu, A viscoelastic nonlinear energy sink with an electromagnetic energy harvester: Narrow-band random response, Chinese Physics B 33 (2024) 070205.

[16] X. Wang, H. Wu, B. Yang, Nonlinear multi-modal energy harvester and vibration absorber using magnetic softening spring, Journal of Sound and Vibration 476 (2020) 115332.

[17] T. Wang, S. Zhu, Analysis and experiments of a pendulum vibration energy harvester with a magnetic multi-stable mechanism, IEEE Transactions on Magnetics 58 (2022) 1–7.

[18] S. Naifar, S. Bradai, O. Kanoun, Design study of a nonlinear electromagnetic converter using magnetic spring, The European Physical Journal Special Topics 231 (2022) 1517–1528.

[19] W. Wang, H. Wei, Z.-H. Wei, Numerical analysis of a magnetic-spring-based piecewise nonlinear electromagnetic energy harvester, The European Physical Journal Plus 137 (2022) 56.

[20] S. Rajasekar, M. A. F. Sanjuán, Nonlinear Resonances, Springer Series in Synergetics, Springer, Switzerland, 2016.

[21] H. Karimpour, M. Eftekhari, Exploiting double jumping phenomenon for broadening bandwidth of an energy harvesting device, Mechanical Systems and Signal Processing 139 (2020) 106614.

[22] Y.-H. Sun, Y.-H. Zeng, Y.-G. Yang, Identification of hybrid energy harvesting systems with non-gaussian process, Acta Mechanica Sinica 40 (2024) 523154.

[23] J. Han, D. Huang, W. Li, G. Yang, N. Gubeljak, Moment analysis of galloping energy harvesters with a parallel circuit under stochastic excitation, International Journal of Non-Linear Mechanics 157 (2023) 104518.

[24] D. Huang, J. Han, W. Li, H. Deng, S. Zhou, Responses, optimization and prediction of energy harvesters under galloping and base excitations, Communications in Nonlinear Science and Numerical Simulation 119 (2023) 107086.
[25] D. Huang, S. Zhou, Z. Yang, Resonance mechanism of nonlinear vibrational multistable energy harvesters under narrowband stochastic parametric excitations, Complexity 2019 (2019) 1050143.
[26] M. Aravindan, S. F. Ali, Array enhanced stochastic resonance for augmented energy harvesting, Communications in Nonlinear Science and Numerical Simulation 111 (2022) 106476.
[27] M. F. Daqaq, Transduction of a bistable inductive generator driven by white and exponentially correlated gaussian noise, Journal of Sound and Vibration 330 (2011) 2554–2564.
[28] P. S. Landa, P. V. E. McClintock, Vibrational resonance, Journal of Physics A: Mathematical and General 33 (2000) L433.
[29] U.E Vincent, P.V.E McClintock, I. Khovanov, S. Rajasekar, Vibrational and stochastic resonances in driven nonlinear systems, 379 (2021) 20200226.
[30] J. Yang, S. Rajasekar, M. A. Sanjuan, Vibrational resonance: A review, Physics Reports 1067 (2024) 1–62.
[31] S. Jeyakumari, V. Chinnathambi, S. Rajasekar, M. A. F. Sanjuán, Analysis of vibrational resonance in a quintic oscillator, Chaos 19 (2009) 043128.
[32] S. Rajasekar, J. Used, A. Wagemakers, M. A. F. Sanjuán, Vibrational resonance in biological nonlinear maps, Communications in Nonlinear Science and Numerical Simulation 17 (2012) 3435–3445.
[33] T. O. Roy-Layinde, J. A. Laoye, O. O. Popoola, U. E. Vincent, P. V. E. McClintock, Vibrational resonance in an inhomogeneous medium with periodic dissipation, Physical Review E 96 (2017) 032209.
[34] K. A. Omoteso, O. Ozioko, O. Bagdasar, T. O. Roy-Layinde, U. H. Diala, Numerical analyses of acoustic vibrational resonance in a helmholtz resonator, Nonlinear Dynamics (2024) 1–21.
[35] M. Coccolo, G. Litak, J. M. Seoane, M. A. F. SanjuÃ¡n, Optimizing the electrical power in an energy harvesting system, International Journal of Bifurcation and Chaos 25 (2015) 1550171.
[36] Y. Jia, Review of nonlinear vibration energy harvesting: Duffing, bistability, parametric, stochastic and others, Journal of intelligent material systems and structures 31 (2020) 921–944.
[37] I. I. Blekhman, Vibrational Mechanics. Nonlinear dynamic effects, general approach, Applications., World Scientific, Singapore, 2000.
[38] M. Brennan, I. Kovacic, A. Carrella, T. Waters, On the jump-up and jump-down frequencies of the duffing oscillator, Journal of Sound and Vibration 318 (2008) 1250–1261.
[39] J. A. Laoye, T. O. Roy-Layinde, K. A. Omoteso, O. O. Popoola, U. E. Vincent, Vibrational resonance in a higher-order nonlinear damped oscillator with rough potential, Pramana-Journal of Physics. 93 (2019) 102.
[40] I. I. Blekhman, P. S. Landa, Conjugate resonances and bifurcations in nonlinear systems under biharmonical excitation, International Journal of Non-Linear Mechanics 39 (2004) 421–426.
[41] K. A. Omoteso, T. O. Roy-Layinde, J. A. Laoye, U. E. Vincent, P. V. McClintock, Delay-induced vibrational resonance in the rayleigh–plesset bubble oscillator, Journal of Physics A: Mathematical and Theoretical 55 (2022) 495701.
[42] H. Yabuno, M. Miura, N. Aoshima, Bifurcation in an inverted pendulum with tilted high-frequency excitation: analytical and experimental investigations on the symmetry-breaking of the bifurcation, Journal of Sound and Vibration 273 (2004) 493–513.
[43] C.-G. Yao, Z.-W. He, M. Zhan, High frequency forcing on nonlinear systems, Chinese Physics B 22 (2013) 030503.
[44] J. J. Thomsen, Effective properties of mechanical systems under high-frequency excitation at multiple frequencies, Journal of Sound and Vibration 311 (2008) 1249–1270.
[45] A. Fidlin, J. J. Thomsen, Non-trivial effects of high-frequency excitation for strongly damped mechanical systems, International journal of non-linear mechanics 43 (2008) 569–578.
[46] I. I. Blekhman, Selected topics in vibrational mechanics, volume 11, chapter: Conjugate Resonances and Bifurcations of Pendulums under Biharmonical Excitation, World Scientific Publishing Company, Singapore, 2004, pp. 151–165.
[47] U. E. Vincent, T. O. Roy-Layinde, O. O. Popoola, P. O. Adesina, P. V. E. McClintock, Vibrational resonance in an oscillator with an asymmetrical deformable potential, Physical Review E 98 (2018) 062203.
[48] T. O. Roy-Layinde, J. A. Laoye, O. O. Popoola, U. E. Vincent, Analysis of vibrational resonance in bi-harmonically driven plasma, Chaos 26 (2016) 093117.
[49] T. O. Roy-Layinde, U. E. Vincent, S. Abolade, O. O. Popoola, J. A. Laoye, P. V. E. McClintock, Vibrational resonances in driven oscillators with position-dependent mass, Philosophical Transactions of the Royal Society A 379 (2021) 20200227.
[50] P. Sarkar, D. Banerjee, S. Paul, D. S. Ray, Method for direct analytic solution of the nonlinear langevin equation using multiple timescale analysis: Mean-square displacement, Physical Review E 106 (2022) 024203.
[51] T. O. Roy-Layinde, K. A. Omoteso, B. A. Oyero, J. A. Laoye, U. E. Vincent, Vibrational resonance of ammonia molecule with doubly singular position-dependent mass, The European Physical Journal B 95 (2022) 80.
[52] T. O. Roy-Layinde, K. A. Omoteso, O. T. Kolebaje, F. O. Ogunmefun, R. A. Fasasi, J. A. Laoye, U. E Vincent, Vibrational resonance in a multistable system with position-dependent mass, Communications in Theoretical Physics 75 (2023) 115602.
[53] O. G. Abamba, O. T. Kolebaje, U. E. Vincent, P. McClintock, Vibrational resonance in bichromatically excited diatomic molecules in a shifted molecular potential, Physical Review E 110 (2024) 034209.
[54] T. O. Roy-Layinde, K. A. Omoteso, U. Diala, J. A. Runsewe, J. A. Laoye, Analysis of vibrational resonance in an oscillator with exponential mass variation, Chaos, Solitons & Fractals 178 (2024) 114310.
[55] K. Oyeleke, O. Olusola, U. E. Vincent, D. Ghosh, P. V. McClintock, Parametric vibrational resonance in a gyroscope driven by dual-frequency forces, Physics Letters A 387 (2020) 127040.
[56] L. Gammaitoni, I. Neri, H. Vocca, Nonlinear oscillators for vibration energy harvesting, Applied Physics Letters 94 (2009) 164102.
[57] K. A. Omoteso, T. O. Roy-Layinde, J. A. Laoye, U. E. Vincent, P. V. E. McClintock, Acoustic vibrational resonance in a rayleigh-plesset bubble oscillator, Ultrasonics Sonochemistry 71 (2020) 105346.
[58] U. E. Vincent, P. V. E. McClintock, I. A. Khovanov, S. Rajasekar, Vibrational and stochastic resonance in driven nonlinear systems part II, Philosophical Transactions of the Royal Society A 379 (2021) 20210003.

Highlights

- Vibrational resonance (VR) is reported in a Duffing-type energy harvester with electromagnetic transduction structure.
- The oscillator is a vibration-based energy harvester with a single degree of freedom, driven by a dual-frequency force.
- The stiffness parameter determined the potential structure and resonance dynamics of the system.
- The average power absorbed was used as the system's performance metric.
- An enhanced vibration energy harvesting system was demonstrated with nonlinearities.
- The results highlight a new approach for the design and optimisation of electromagnetic energy harvesters.

Authors statement

K. A. Omoteso: Methodology, Data Curation, Visualization, Software, Validation, Investigation, Formal analysis, Writing - Original Draft.

T. O. Roy-Layinde: Software, Validation, Formal analysis, Supervision, Writing - Original Draft, Writing- Reviewing and Editing.

U. H. Diala: Conceptualization, Methodology, Investigation, Software, Formal analysis, Resources, Project administration, Supervision, Writing- Reviewing and Editing.

Declaration of interests

☒ The authors declare that they have no known competing financial interests or personal relationships that could have appeared to influence the work reported in this paper.

☐ The authors declare the following financial interests/personal relationships which may be considered as potential competing interests: